Korean J. Chem. Eng., **25**(3), 395-401 (2008)

CFD modeling of the effect of absorbent size on absorption performance of a packed bed column

Masoud Rahimi† and Mohsen Mohseni

CFD research center, Chemical Engineering Department, Razi University, Kermanshah, Iran
(*Received 20 February 2007 • accepted 18 September 2007*)

Abstract−This paper reports a study on the ability of the computational fluid dynamics (CFD) modeling for analyzing the fluid flow hydrodynamics and absorption in a packed bed column. The water absorption by silica gel absorbents in an experimental packed bed was investigated, and the absorption performance of two different sizes of absorbent was studied. A series of experiments were carried out for five setups which are different in the weight ratio of the employed big to small absorbents. The CFD modeling was carried out for all five experimental setups. The predicted results show that by more replacing of the big absorbents with the small ones the water absorption increased. On the other hand, a greater pressure drop was observed as more small absorbents were used. The predicted absorption rates were compared with the measured values and on average a consistency within 11.6% was observed.

Key words: Absorption, Computational Fluid Dynamics, Modeling, Packed Bed, Column

INTRODUCTION

Fixed beds are widely used in a number of chemical industries processes. Examples are provided by adsorption, reactive separation and heterogeneous catalysis in chemical reactors. In the solid fixed and fluidized bed columns all three transfer phenomena including fluid, mass and heat transfer are very important. Besides the importance of the mass transport inside the porous catalyst, the external resistance to the mass transfer, which is usually defined by the mass transfer coefficient, strongly depends on the flow fluid field around the particles. Most researches have tried to experimentally and theoretically determine the effect of fluid flow on the fixed or fluidized performance [1,2].

By development of computers and increasing of their simulation power, numerical modeling has been preferred in many cases to expensive experiments [3]. The CFD studies can improve our understanding about the fluid flow, heat and mass transfer inside the fixed beds. In using CFD for modeling of fixed bed columns, the geometrical complexity of the packing demands more computation. Therefore, the approach can so far have been applied only to a small section of a column. In CFD modeling of fixed beds, the geometric modeling and grid generation are more complicated than modeling of other processes [4].

In all types of CFD modeling, two factors determine the difficulty of modeling: the number of objects in the model and the number of control volumes. In a packed bed the amount of packing and the narrow region between them makes its modeling more complicated. By reviewing most of research done for this purpose, it can be found that there are difficulties in modeling of packing due to limitations in computer processing power.

Much research in this field has been focused on the pressure drop and fluid flow hydrodynamics around the catalyst [5,6], while some other research was interested in the mass, heat transfer and temperature field inside the reactor [7].

The CFD predicted pressure drop and heat transfer was compared with the experimental results by Calis et al. [8] and a good agreement between these results was reported. It was shown that the CFD with an error of 10% could be used to predict the pressure drop across beds of spheres that have a channel-to-particle diameter ratio of 2. In their study, the predicted local velocity profile on a cross-section of the packed bed was compared with that measured with the LDA and a good agreement was reported.

The relationship between the local flow field and wall heat flux in a packed bed of spheres was studied by Nijemeisland and Dixon [9]. The CFD was used for obtaining the velocity and temperature fields for gas flowing through a periodic wall segment test cell. They showed that the local patterns of wall heat flux are related to larger-scale flow structures in the bed and did not correlate statistically with the local flow field. In their modeling, the actual contact points were eliminated in order to facilitate turbulent solution of the model. They found using a sphere diameter of 99% of the actual sphere diameter allowed a turbulent solution to be obtained and the original velocity distribution around the contact points maintained properly.

In continuation of this study, an investigation was carried out by Nijemeisland et al. [10] to find the influence on heat transfer performance in the near-wall region of internal voids of cylindrical particles in a steam reforming packed bed reactor. The CFD modeling was used to obtain the detailed flow and temperature fields in a representative wall segment of the tube. They showed that particles without internal voids performed better than particles with internal voids in the bed interior.

Guardo et al. [11] presented a numerical modeling of particle-to-fluid heat transfer in fixed beds by using a CFD solver. In their study, two different configurations of forced convection at low pressure and combination of free and forced convection at high pressure with supercritical CO_2, as circulating fluid, were studied. The obtained numerical results were compared with previously published data.

The present study has tried to introduce CFD modeling of a packed bed containing up to 5000 catalysts. This work has not the preci-

†To whom correspondence should be addressed.
E-mail: masoudrahimi@yahoo.com

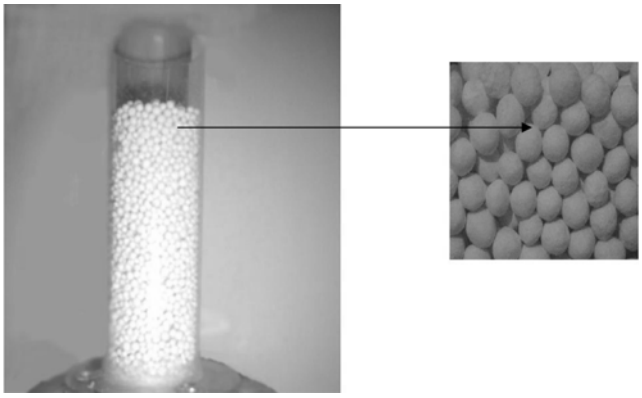

Fig. 1. The column and the small size absorber.

sion of the previous studies which were done for a limited number of catalysts or granules [10-12], but it is useful for understanding the fluid flow hydrodynamics inside the whole bed. In other words, this work illustrates the ability of the CFD for analyzing packed bed columns with modeling of the whole column instead of a local study of the bed's packing. In the present modeling, various process parameters such as pressure, velocity, temperature, absorption rate, etc., were predicted inside the whole bed.

EXPERIMENTS

The experimental rig consists of a column and a one-liter reservoir equipped with a 1,000 W heater, which is able to produce 0.36 gr/s steam. The generated steam enters a Perspex cylindrical column having a diameter of 4.6 cm and a height of 15 cm. The cylinder was filled with water absorber silica gel granules. Two sizes of 3 mm and 6 mm of granules were used in the experiments.

Fig. 1 shows the filled column with the small size silica gel absorbent. The big and small absorbent had the same density of 1.45 gr/cm^3 while the small absorbent had a surface area of 1.4 m^2 per kilogram of its weight, and this value for the big one was 0.7.

In order to find how the absorbent granules are saturated with steam, a stream of steam was passed upon 10 granules placed in one row. The water absorption progress by 3 mm and 6 mm granules in various time steps is shown in Fig. 2. In this figure, the absorption progress is expressed by the mass water absorbed per unit surface as well as per unit weight of absorbents.

The figure illustrates significant differences in the performances of the absorbents as the absorption expressed by water absorbed per weight of absorbent. It can found that the absorption by the small absorbent is higher than that measured for the large one due to its higher available surface area. However, the water absorbed per unit surface is almost similar for both sizes during first 8 s, which corresponds to water absorption of 50 gr/m^2. Therefore, in this range it is possible to say that the absorption behavior just depends on the surface area and is independent of the absorbents' size. Regarding this result, all the experiments were performed in a way that the amount of absorption was to be less than this value.

Five experimental sets were carried out and in all experiments the column was filled with 180gr of absorbent as follows:

a) 180 gr of small absorbent.

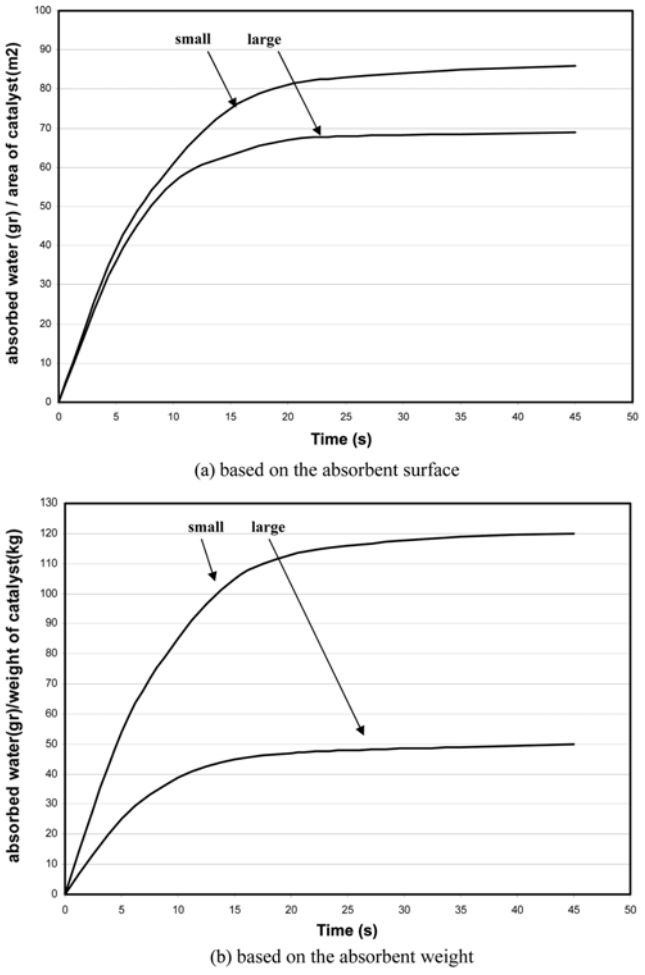

Fig. 2. Absorption progress by the small and large-sized absorbents.

Table 1. The overall absorbed water at different setups

% small	Catalyst weight (gr)	Small catalyst height (cm)	Large catalyst height (cm)	Absorbed water (gr/s)
0	180	0.0	13.0	0.121
33	180	4.2	8.7	0.133
55	180	6.9	5.8	0.144
61	180	7.8	4.8	0.150
100	180	12.5	0.0	0.176

b) 180 gr of large absorbent.

c) 60 gr of small absorbent & 120 gr of large absorbent.

d) 100 gr of small absorbent & 80 gr of large absorbent.

e) 110 gr of small absorbent & 70 gr of large absorbent.

Each experiment was repeated three times and the averaged absorption rates are reported in Table 1. As illustrated in the table, by replacing the big absorbent with the small one the overall absorption rates increased due to increasing of the available surface for the water absorption. These results show that with replacing the whole bed with the small absorbent the absorption rate increased by 45%.

In addition, a separate run was performed to find the differences in the absorption rate of granules placed at different regions inside the bed. In this experiment, four small granules were marked and

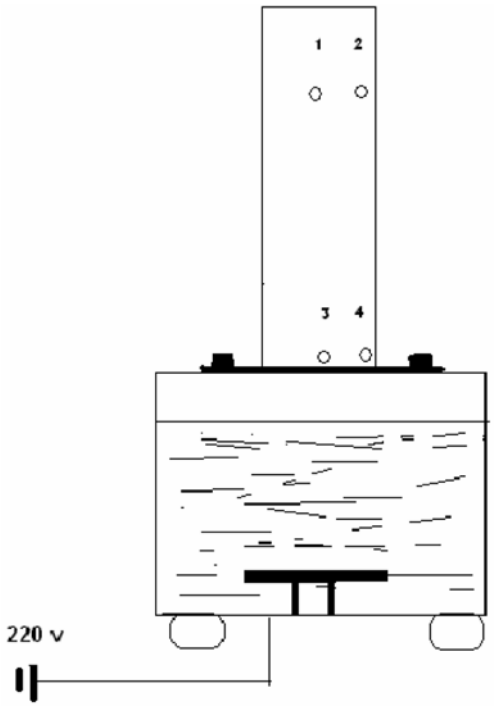

Fig. 3. A schematic view of the position of the four marked absorbents.

placed inside the packed bed of small granules at two levels, which are the bottom of the bed and 7 cm from the bottom, as illustrated in Fig. 3. At each level, one of the absorbents was placed at the column center line and the other one close the column's wall. The results show after 60 s that almost 40% more water was absorbed by the absorbents placed at the bottom. In addition, the results show that the difference between water absorption by points 1 and 2 is higher than that of points 3 and 4. The absorbent placed close to the wall at point 2 absorbed almost 70% more water than the absorbent placed at point 1 at the middle of the column.

MODELING

The CFD modeling involves the numerical solution of conservation equations. In this work, the simultaneous solution of continuity and Reynolds-averaged Navier-Stokes (RANS) equations together with the k−ε turbulence model were carried out and the following equations are used in the model [13]:

Continuity equation

$$\mathrm{div}\mathbf{U}=0 \tag{1}$$

Momentum equations

$$\frac{\partial u}{\partial t}+\mathrm{div}(u\mathbf{U})=-\frac{1}{\rho}\frac{\partial p}{\partial x}+\nu\,\mathrm{div}(\mathrm{grad}\,u)+\left[-\frac{\partial\overline{u'^2}}{\partial x}-\frac{\partial\overline{u'v'}}{\partial y}-\frac{\partial\overline{u'w'}}{\partial z}\right]+S_{Mx} \tag{2}$$

$$\frac{\partial v}{\partial t}+\mathrm{div}(v\mathbf{U})=-\frac{1}{\rho}\frac{\partial p}{\partial y}+\nu\,\mathrm{div}(\mathrm{grad}\,v)+\left[-\frac{\partial\overline{u'v'}}{\partial x}-\frac{\partial\overline{v'^2}}{\partial y}-\frac{\partial\overline{v'w'}}{\partial z}\right]+S_{My} \tag{3}$$

$$\frac{\partial w}{\partial t}+\mathrm{div}(w\mathbf{U})=-\frac{1}{\rho}\frac{\partial p}{\partial z}+\nu\,\mathrm{div}(\mathrm{grad}\,w)+\left[-\frac{\partial\overline{u'w'}}{\partial x}-\frac{\partial\overline{w'v'}}{\partial y}-\frac{\partial\overline{w'^2}}{\partial z}\right]+S_{Mz} \tag{4}$$

and for a scalar quantities:

$$\frac{\partial\Phi}{\partial t}+\mathrm{div}(\Phi\mathbf{U})=\mathrm{div}(\Gamma_{\Phi}^{*}\mathrm{grad}\,\Phi)+\left[-\frac{\partial\overline{u'\varphi'}}{\partial x}-\frac{\partial\overline{v'\varphi'}}{\partial y}-\frac{\partial\overline{w'\varphi'}}{\partial z}\right]+S_{\Phi} \tag{5}$$

Which in general notation:

$$-\rho\overline{u_i'\varphi'}=\Gamma_t\frac{\partial\Phi}{\partial x_i}$$

$$-\rho\overline{u_i'u_j'}=\tau_{ij}=\mu_T\left(\frac{\partial u_i}{\partial x_j}+\frac{\partial u_j}{\partial x_i}\right) \tag{6}$$

A turbulence model is a computational procedure to calculate μ_T. The Reynolds stress terms, u_i' and u_j', can be defined on the basis of time-averaged velocity component.

In order to involve the effect of the turbulence model on the predicted results three models were employed. The models were selected from the two equation k−ε family model including the standard [14], RNG [15] and realizable [16]. The two-equation k−ε model consists of an equation for the turbulent kinetic energy, k, and the other for the energy dissipation rate, ε, as described in the following equations:

$$\frac{\partial(\rho k)}{\partial t}+\frac{\partial}{\partial x_i}(\rho u_i k)=\frac{\partial}{\partial x_i}\left(\rho\frac{\nu_{eff}}{\sigma_k}\frac{\partial k}{\partial x_i}\right)+\rho(P_k-\varepsilon) \tag{7}$$

$$\frac{\partial(\rho\varepsilon)}{\partial t}+\frac{\partial}{\partial x_i}(\rho u_i\varepsilon)=\frac{\partial}{\partial x_i}\left(\rho\frac{\nu_{eff}}{\sigma_\varepsilon}\frac{\partial\varepsilon}{\partial x_i}\right)+S_\varepsilon \tag{8}$$

and:

$$\mu_T=\rho C_\mu\frac{k^2}{\varepsilon} \tag{9}$$

which:

$$\nu_{eff}=\frac{\mu_{eff}}{\rho}\ \text{ and }\ \mu_{eff}=\mu+\mu_T \tag{10}$$

The standard k−ε model is a semi-empirical model based on transport equations for the turbulent kinetic energy (k) and its dissipation rate (ε). As the strengths and weaknesses of the standard k−ε model have become known, improvements have been made to the model to improve its performance by the RNG and Realizable models.

In the RNG k−ε model, the effect of small-scale turbulence is represented by means of a random forcing function in the Navier-Stokes equations. The RNG procedure systematically removes the small scales of motion from the governing equations by expressing their effects in terms of larger-scale motion and a modified viscosity. The realizable k−ε model is a relatively recent development and contains a new formulation for the turbulent viscosity and a new transport equation for the dissipation rate, ε. It has been derived from an exact equation for the transport of the mean-square vorticity fluctuation. Both the realizable and RNG k−ε models have shown substantial improvements over the standard k−ε model where the flow

Table 2. The definition in family turbulence models

Model	S_ε	Parameters
Standard Launder and Spalding [14]	$\rho\left(C_{1,S}\frac{\varepsilon}{k}P_k - C_{2,S}\frac{\varepsilon}{k}\varepsilon\right)$	$C_{\mu,s}=0.09$; $C_{1,S}=1.44$; $C_{2,S}=1.92$; $\sigma_{k,S}=1$; $\sigma_{\varepsilon,S}=1.314$
RNG Yakhot, and Orszag [15]	$\rho\begin{pmatrix} C_{1,RNG}\frac{\varepsilon}{k}P_k - \alpha\frac{\varepsilon}{k}\varepsilon \\ -C_{2,RNG}\frac{\varepsilon}{k}\varepsilon \end{pmatrix}$	$\alpha=C_\mu\eta^3\frac{1-\eta/\eta_0}{1+\beta\eta^3}$, $C_{\mu,RNG}=0.0845$; $C_{1,RNG}=1.42$; $C_{2,RNG}=1.68$; $\sigma_{k,RNG}=\sigma_{\varepsilon,RNG}=0.719$; $\eta_0=4.8$; $\beta=0.012$ $\eta=E\frac{k}{\varepsilon}$; $E^2=2E_{ij}E_{ij}$; $E_{ij}=0.5\left(\frac{\partial u_i}{\partial x_j}+\frac{\partial u_j}{\partial x_i}\right)$
Realizable Shih et al. [16]	$\rho\left(C_{1,Re}E\varepsilon - C_{2,Re}\frac{\varepsilon^2}{k+\sqrt{\nu\varepsilon}}\right)$	$C_{1,Re}=\max\left[0.43;\frac{\eta}{\eta+5}\right]$; $C_{\mu,Re}=0.09$; $C_{2,Re}=1.9$; $\sigma_{k,Re}=1$; $\sigma_{\varepsilon,Re}=1.2$ $\eta=E\frac{k}{\varepsilon}$; $E^2=2E_{ij}E_{ij}$; $E_{ij}=0.5\left(\frac{\partial u_i}{\partial x_j}+\frac{\partial u_j}{\partial x_i}\right)$

features include strong streamline curvature, vortices, and rotation.

As can be seen in Eqs. (7), (8), the relations are the same as the general transport equations, with the source terms, s_ε, defined in different ways for each model. Table 2 illustrates the s_ε relations for the k–ε family models. The relation for p_k has been defined as follows:

$$P_k = \nu_t\left(\frac{\partial u_i}{\partial x_j}+\frac{\partial u_j}{\partial x_i}\right)\frac{\partial u_i}{\partial x_j} \tag{11}$$

In preparing the geometry, the modeling domain includes a cylinder with a diameter of 4.6 cm, and a height of 15 cm was meshed into almost 300000 to12000000 number of tetrahedral cells according to the ratio of the big to small absorbents. The segregated type of solver in three dimensions was used. The simple pressure-velocity coupling algorithm, the standard pressure, the first order upwind discretization scheme for momentum, energy, turbulent kinetic energy and dissipation energy were employed in the model. A conversion criterion of 10^{-7} was chosen for all parameters.

The saturated steam was passed theoretically through the tube with a temperature of 100 °C and mass flow rate of 0.36 gr/s according to the experimental setting. The cylinder was filled with small and large sized spheres according to real experimental setups. In order to making the geometry closer to a real case, a row of the pellets was configured in a random pattern and the next row with was rotated by 60°. This pattern was repeated every three rows in the model. Fig. 4 illustrates the column and an example of its meshed configuration.

RESULTS

By simultaneous solving of the above-mentioned equations over the whole domain, the velocity fluid flow and the other hydrodynamics parameters were obtained. In order to show the importance

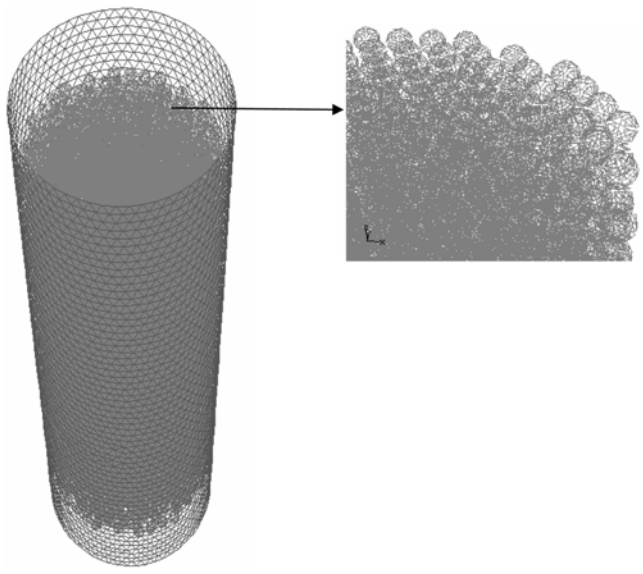

Fig. 4. The meshed column and absorbents.

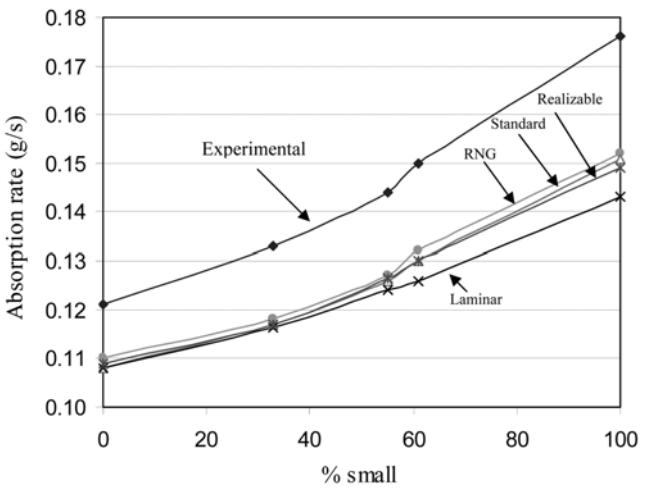

Fig. 5. A comparison between the experimental and predicted results using different versions of k–ε model and the laminar condition assumption.

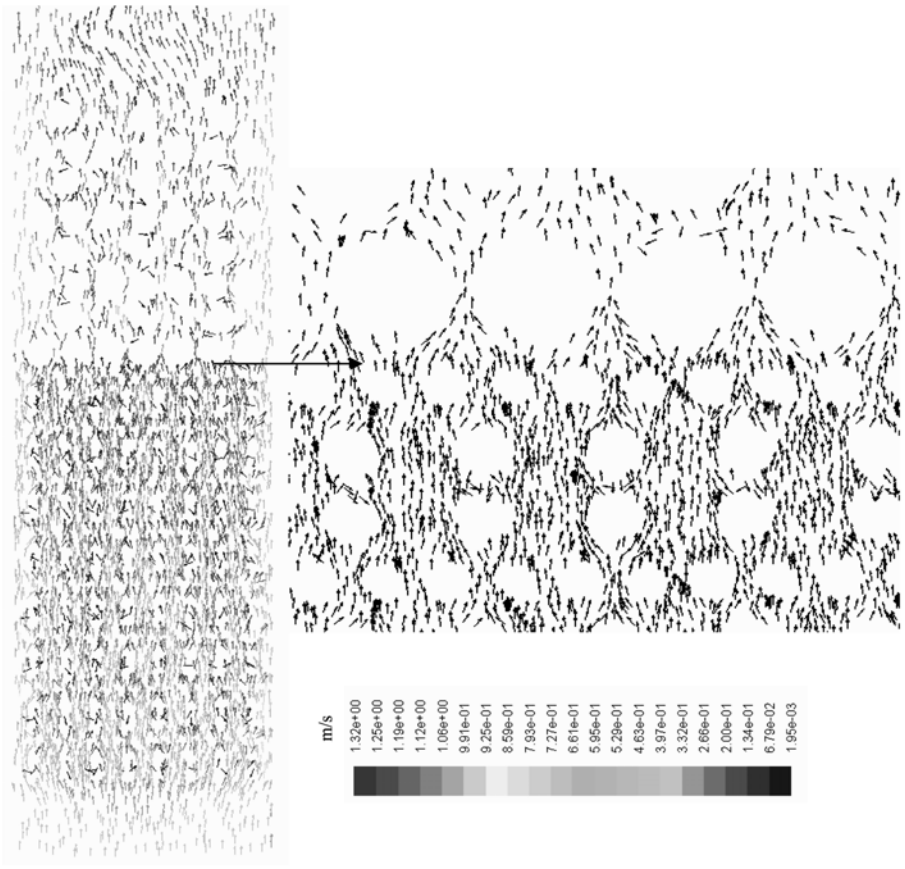

Fig. 6. The velocity vectors field in a vertical slice.

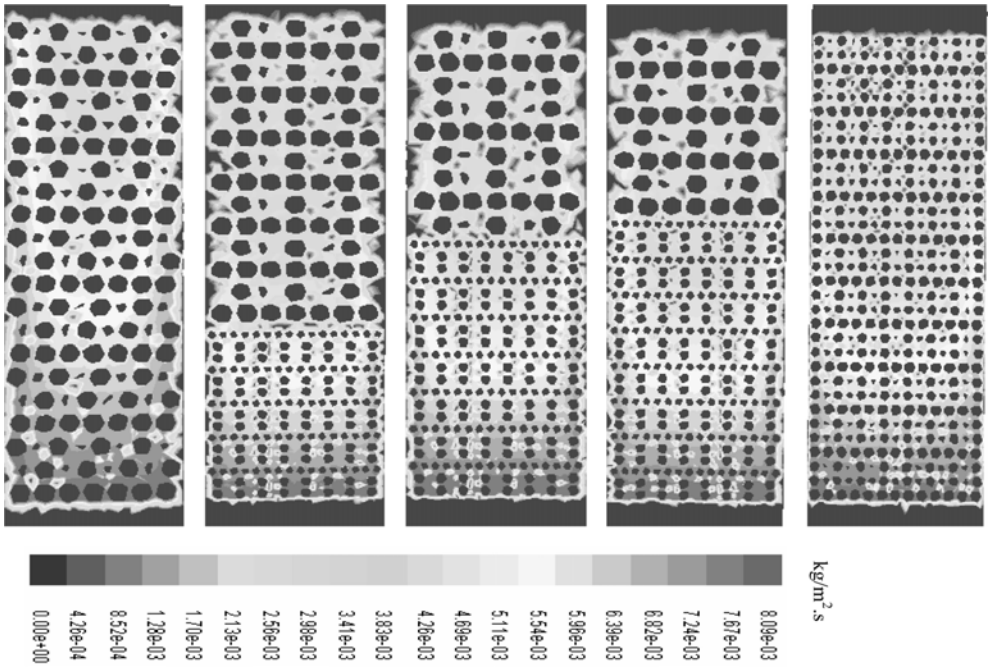

Fig. 7. The contour plots of absorption rate in a vertical slice.

of considering the fluid turbulence and the effect of using different turbulence models on predicted results, the model was run by using the standard, RNG and realizable versions of the k–ε model. In addition, the flow regime was assumed to be laminar in order to investigate the importance of employing the turbulence models in the modeling. Fig. 5 illustrates the predicted absorption rates at various ratios

of the small to big granules by using different turbulence models as well as in the laminar condition. The results show that the importance of employing the turbulence model increased as more small absorbent was used in the bed. However, the differences between the obtained values using a different version of k–ε turbulence model are not significant. The RNG model was selected as the turbulence model in the present work as its predictions were closer to the absorption rate measured values.

Fig. 6 shows that the predicted vector plot in a vertical slice goes through the middle of the column for the 55% small absorbent setup. The velocity vector shows that the steam stream enters the column, and after hitting the absorbents its velocity increases due to decreasing of the passage route. The higher velocity close to the wall can be explained by more available space for the steam movement.

Fig. 7 illustrates the rate of absorption rate per unit area in the above-mentioned slice for five different setups. The figure shows that in all setups the rate of absorption of steam at the beginning of the column is higher due to the higher available steam. This rate is reduced as the steam is absorbed by the absorbents in a way that the lowest value can be found at the outlet region of the column. The figure also illustrates that in all setups the absorption rate is lower at the middle of the column in comparison with that of the lateral sides. This is in agreement with the measured results in the experimental part of this study for four selected points shown in Fig. 3. The results show that the absorption rate fields are different in various setups as the large-sized absorbents are replaced by the small one. The figure shows the absorption rate per unit area in the full large size setup has higher values in comparison with the other setups. This can be explained with the higher concentration of the steam throughout for this setup due to lower performance of the large-sized absorbent. In other words, at the beginning of the column in which the water was absorbed by the small granules in a more efficient way, the steam concentration decreased faster. Therefore, due to the lower concentration of the available steam the absorption rate is lower at the top region. However, the overall predicted absorptions are higher in the cases that more small absorbents were employed. This is in agreement with the experimental observation. Complementary contour plots of the absorption rate at six horizontal slices placed at different levels of the column filled with 55% small granules are shown in Fig. 8. The figure illustrates the reduction of the rate of absorption from the wall toward the column's center as well as from the bottom to the top. In addition, the figure illustrates the change in the absorption rate pattern as the fluid enters the large region.

In order to show the consistency and validity of the CFD results, the measured and predicted values of the absorption rate in different geometries are compared in Table 3. The predicted values show a maximum error of 13.6% and an average error value of 11.6%. The error increases as the size of particles decreases, which can be explained by deficiency of the turbulence model in predicting the turbulent flow established inside the bed.

Both the experimental and CFD results show that the small-sized absorbent works in a more efficient way in comparison with the big one. However, the pressure drop caused by different layouts

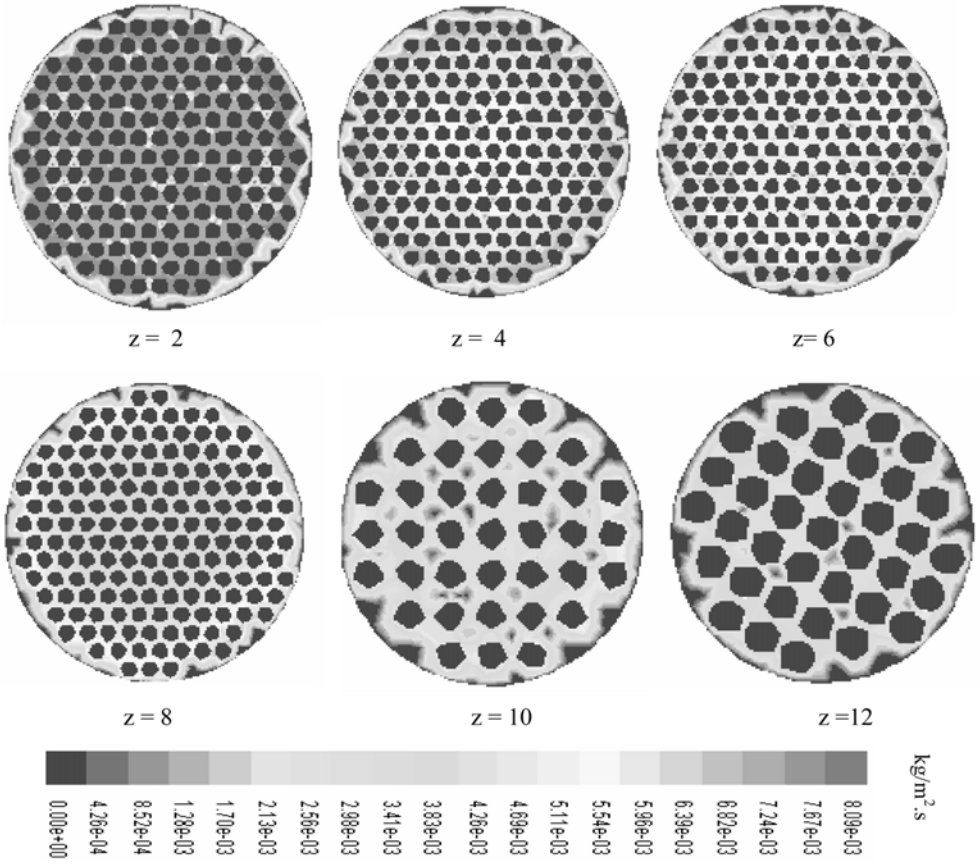

Fig. 8. The absorption rate at different distances (cm) from the column's bottom.

Table 3. The comparison between the measured and predicted overall absorption rates

% small	Exp (g/s)	CFD (g/s)	% error
0	0.121	0.110	9.1
33	0.133	0.118	11.3
55	0.144	0.127	11.8
61	0.150	0.132	12.0
100	0.176	0.152	13.6

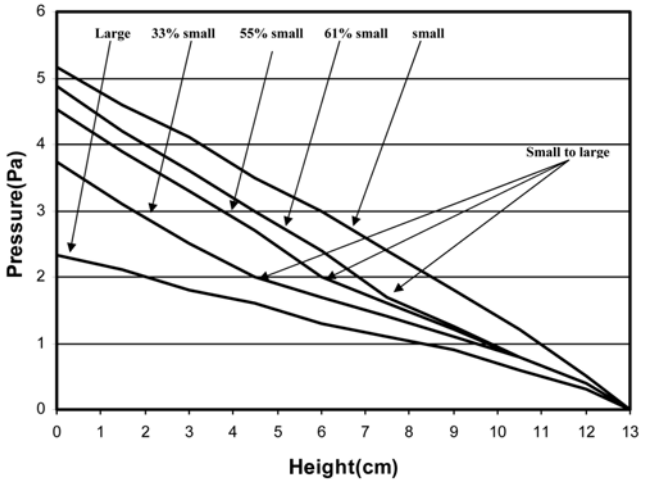

Fig. 9. The predicted pressure drops across the column.

can be important from the economical aspect. Fig. 9 shows the predicted pressure drops across the bed for the five setups. The results show that more pressure drops are expected as the large absorbent is replaced with the small one. The predicted pressure drop in the full large granule setup is almost half of that caused by the full small absorbent layout. In addition, in the layouts that consist of two different sizes of absorbent, the slope of the pressure line is lower in the large granules region in comparison with the small absorbent domain.

As illustrated above, the pressure drop increases as we try to reach more absorption. In other words, to access more absorption a higher cost must be paid in order to overcome the higher pressure drop. By using the CFD predictions, it will be convenient to determine the optimum ratio of the small to big size absorbent weight in fixed bed columns. In addition, the predicted fluid flow hydrodynamics, heat and mass transfer can be a useful tool in determining the performance of the system and avoiding expensive experiments in real scales.

CONCLUSIONS

1. CFD modeling can be a useful tool to improve our knowledge about heat/mass and fluid flow hydrodynamic in packed beds.
2. The CFD predicted result on a packed bed could be used for determining active regions in the packed beds.
3. The CFD prediction can be used for analyzing the experimental observation of the absorption process in a packed bed.
4. The CFD can be useful for right decision about the employed size of packing in a packed bed.

ACKNOWLEDGMENT

The authors wish to express their thanks to the Abadan Refinery of Iran for the financial support of this work.

NOMENCLATURE

C_1, C_2, C_μ : constants of the k–ε model
E_{ij} : linear deformation rate [s^{-1}]
G : dissipation function [Pa s^{-1}]
S : source term
U : velocity vector [m s^{-1}]
k : turbulent kinetic energy [J kg^{-1}]
u, v, w, u_i, u_j : mean velocity components [m s^{-1}]
u′, v′, w′, u_i', u_j' : turbulent fluctuating velocity components [m s^{-1}]
x_i, x_j : Cartesian coordinate [m]

Greek Letters

ε : dissipation rate of k [w kg^{-1}]
μ, μ_T, μ_{eff} : laminar, turbulent and effective viscosity [Pa s]
ν, ν_T, ν_{eff} : laminar, turbulent and effective kinematic viscosity [$m^2 s^{-1}$]
ρ : density [kg m^{-3}]
σ_k, σ_ε : turbulent Prandtl numbers for k–ε
Φ, φ' : mean and turbulent fluctuating values of scalar property
Γ : scalar diffusion coefficient

REFERENCES

1. H. I. Cho, C. H. Chung, G. Y. Han, G. R. Ahn and J. S. Kong, *Korean J. Chem. Eng.*, **17**, 292 (2000).
2. C. K. Yi, S. H. Jo, B. H. Lee, S. Y. Lee, J. E. Son and G. T. Jin, *Korean J. Chem. Eng.*, **18**, 1005 (2001).
3. S. B. Lee, W. Cho, D. K. Park and E. S. Yoon, *Korean J. Chem. Eng.*, **23**, 522 (2006).
4. V. Ranade, *Computational flow modeling for chemical reactor engineering*, Academic Press, New York (2002).
5. J. Tobis, *Ind. Eng. Chem. Res.*, **41**, 2552 (2002).
6. P. Magnico, *Chem. Eng. Sci*., **58**, 5005 (2003).
7. S. J. P. Romkes, F. M. Dautzenberg, C. M. van den Bleek and H. P. A. Calis, *Chem. Eng. J*., **96**, 3 (2003).
8. H. P. A. Calis, J. Nijenhuis, B. C. Paikert, F. M. Dautzenberg and C. M. van den Bleek, *Chem. Eng. Sci*., **56**, 1713 (2001).
9. M. Nijemeisland and A. G. Dixon, *AIChE J*., **50**, 906 (2004).
10. M. Nijemeisland, A. G. Dixon and E. H. Stitt, *Chem. Eng. Sci*., **59**, 5185 (2004).
11. A. Guardo, M. Coussirat, F. Recasens, M. A. Larrayoz and X. Escaler, *Chem. Eng. Sci*., **61**, 4341 (2006).
12. S. A. Logtenberg, M. Nijemeisland and A. G. Dixon, *Chem. Eng. Sci*., **54**, 2433 (1999).
13. H. K. Versteeg and W. Malalasekera, *An introduction to computational fluid dynamics, the finite volume method*, Longman Limited, England (1995).
14. B. E. Launder and D. B. Spalding, *Mathematical models of turbulence*, Academic Press, England (1974).
15. V. Yakhot and S. A. Orszag, *J. Sci. Comput*., **1**, 1 (1986).
16. T. H. Shih, W. W. Liou, A. Shabbir and J. Zhu, *Comput. Fluids*, **24**, 227 (1995).